



Mechanical Behavior of Seamless Pipes Using Ring Expansion Technique and Novel Hoop Stress Correlation Factor (K)

K. Abdelgawad¹ · A. Nassef^{1,2} · Mohamed T. Eraky³ · M. Saber^{1,4}

Received: 17 April 2023 / Accepted: 4 October 2023
© The Author(s) 2023, corrected publication 2023

Abstract

This study investigated the stress–strain behavior of seamless pipes in the hoop direction using the ring expansion test, which is a non-standardized mechanical testing technique used for evaluating the mechanical properties of round tubes. However, this technique has limitations, such as unidentified specimen geometry, strain measurement, and the estimation of friction coefficients. The study employed experimental, numerical, and analytical methodologies to address these limitations and throughout the study, a novel hoop stress correlation factor (K) was identified to be multiplied by the hoop stress derived equation for reduced section ring specimens. The experimental strain was measured using a newly derived analytical equation, and a mathematical predictive model was developed to estimate the K-factor using the Design of Experiment (DoE) and Design-Expert statistical software. The study concluded that the ring expansion test is a promising technique for evaluating the mechanical properties of seamless pipes similar to the unified axial tensile stress–strain behavior. However, future research is needed to estimate the hoop stress correlation value (K) for all ring geometries. The study's finding of the novel hoop stress correlation factor (K) in the case of a reduced section ring specimen is particularly noteworthy, as it addresses a significant research gap in the field.

Keywords Ring expansion test · Hoop stress · FEA · Thin cylinders · Material characterization

Introduction

ASTM A106 grade B Seamless Pressure Pipe (ASME SA106) is a widely used material in industries such as oil and gas refineries, power stations, petrochemical factories, ships, and other facilities where high-pressure and high-temperature fluids and gases are transported [1]. To ensure the optimum usage of this pipe, it is essential to investigate its mechanical properties. While conventional mechanical testing methods such as tensile, 3-point bending, and creep tests have been standardized by various organizations, non-conventional techniques are being developed to simulate the working conditions of the pipe in service or when the available material is limited.

One of these non-conventional techniques is the ring tensile test, which involves the use of two D-shaped blocks (mandrels) fitted into the ring and opposite forces applied to the D-blocks until the ring ruptures. Researchers such as Ktari et al. [2], Frolov et al. [3], Gurovich et al. [4], and Yoon et al. [5] have studied this technique. Barsoum et al. [6] used two mandrel designs: one with lubricated D-shaped blocks and the other using lubricated D-shaped blocks with

✉ K. Abdelgawad
k.abdelgawad95@eng.psu.edu.eg

A. Nassef
nassef12@eng.psu.edu.eg

Mohamed T. Eraky
mteraky@mans.edu.eg

M. Saber
msaber@kfu.edu.sa

¹ Department of Production Engineering and Mechanical Design, Faculty of Engineering, PortSaid University, Port Fouad City St. No.12, Portsaid 42526, Egypt

² High Institute of Electronic Engineering, K 10 Bilbies, 10th Ramadan, Egypt

³ Production Engineering and Mechanical Design Department, Faculty of Engineering, Mansoura University, Mansoura 35516, Egypt

⁴ Department of Mechanical Engineering, College of Engineering, King Faisal University, 31982 Al-Ahsaa City, Saudi Arabia

needle roller bearing (which decreased friction coefficient into $\sim 50\%$ of its value upon using needle bearing), also further investigation was carried out to optimize the ring specimen with a reduction in its cross-section to maintain a uniform stress distribution along the gauge length and give a fracture at the center of the specimen. Khalfallah et al. [7] proposed five new designs that incorporate cylindrical rolling bearings, introduce grooves to the mandrel's external lateral area to reduce friction at the ring/mandrel interface. Saber et al. [8], Sultan et al. [9], and Calaf-Chica et al. [10] suggested using smaller cylindrical pins instead of bulk mandrels to minimize friction. Furthermore, the authors succeeded to determine yield and ultimate strength of isotropic seamless pipe in addition to the elastic modulus and the plastic stress–strain property using the ring elongation testing technique [11].

Another non-traditional method is the burst test, which involves introducing a pressurized fluid into a ring specimen for a specific period while gradually increasing the pressure until the specimen fails [12]. The burst creep test is a development that includes a heating chamber around the ring specimen. These tests generate accurate data that simulate the actual working conditions where the material fails at its weakest point. Seok et al. [13] conducted a study comparing the burst creep test and the ring tensile test with an intermediate dog bone insert, and the study revealed identical results between the two techniques.

Jiang et al. [14–16] conducted extensive research on zirconium-based alloy cladding for nuclear fuel using the ring expansion testing technique, which involves using the wedge effect between a cone and a mandrel. This technique is considered an alternative to the burst test, replacing pressure from fluids with pressure from solid rigid parts. Saber et al. [17] further developed this technique by using two cones, which reduced friction interfaces from three to two values and suggested partitioning the mandrel into a minimum of six equal parts to maintain consistent results. Abdelgawad et al. [18] studied the effect of metal-to-metal contact friction and developed a relationship to describe the percentage of pressure dissipation due to friction as a function of mandrel parts.

This study presents an intensive experimental and numerical investigation of the bi-cone wedge ring expansion technique. The testing system includes a mandrel partitioned into four or eight equal parts and two cones assembled from top and bottom. A ring specimen with a reduced cross-section is mounted around the mandrel, which expands radially in response to the cone's axial displacement. This work aims to evaluate the stress–strain properties of the pipe in the hoop direction and correlate the proposed technique results with the standard tensile test results in terms of stress–strain data. This is achieved through a combination of axial load–displacement data

obtained from either the experimental or simulation work in conjunction with the derived theoretical equations. The friction coefficient at the metal-to-metal interfaces is an essential parameter in the evaluation of hoop stress–strain properties and was estimated by comparing experimental data with FE results for different values of the friction coefficients since it is challenging to measure experimentally. In addition, the effect of the specimen's geometry on the resulting data was investigated as well.

Theoretical Analysis

An analytical derivation was conducted to express the internal pressure acting on the ring specimen and the corresponding hoop stress (σ_θ) induced as a function of the applied axial load (F). Additionally, the radial dilation (X_r) and the hoop strain (ϵ_{hoop}) in the ring as a function of the axial displacement (X_a) were determined. The proposed testing technique is illustrated in Fig. 1, while the geometry of the testing system components, including the ring specimen, is

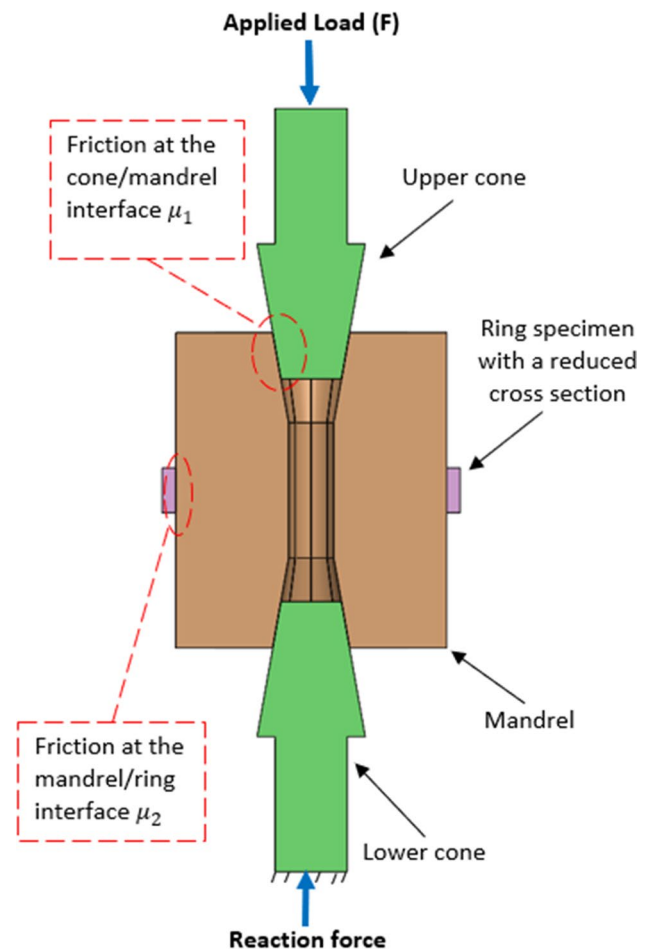


Fig. 1 Ring expansion testing schematic

Table 1 Chemical compositions of the ASTM A106 grade B carbon steel pipe by the manufacturer

Element percentage (%)		C	Mn	P	S	Si	Cr	Cu	Mo	Ni	V
		0.3*	0.29–1.06	0.035*	0.035*	0.1**	0.4*	0.4*	0.15*	0.4*	0.08*
		*Maximum percentage					**Minimum percentage				

depicted in Fig. 4. Saber et al. [17] and Abdelgawad et al. [18] derived an equation to explain the hoop stress generated in the full-ring (without any reduction in its height), which is presented as Eq. (1) [14]. It is worth noting that all symbols used for this derivation match with Saber et al. [17] where they are visualized as well [17].

$$\sigma_{\theta} = \frac{Pd}{2t} = \frac{P'(1-\alpha)d}{2t} = (1-\alpha) \frac{Fd}{At} \left(\frac{1 - \mu_1 \tan\left(\frac{\theta}{2}\right)}{\mu_1 + \tan\left(\frac{\theta}{2}\right)} \right) \quad (1)$$

where (α) is the pressure dissipation factor (due to the friction between the mandrel and the ring), (d) the ring's internal diameter, (A) the internal lateral area of the ring, (t) the

ring's thickness, (μ_1) friction coefficient at the cone/mandrel interface, (P) and (P') are the actual and the nominal internal pressure induced to the ring, and ($\frac{\theta}{2}$) is the cone half angle.

Hence, by using the same principle of studying force analysis (see Appendix section) and by analogy, a displacement analysis would be performed to describe the diametral displacement X_d as in Eq. (2).

$$X_d = 2X_a \left(\frac{1 - \mu_1 \tan\left(\frac{\theta}{2}\right)}{\mu_1 + \tan\left(\frac{\theta}{2}\right)} \right) \quad (2)$$

And since the radial displacement X_r could be evaluated as $X_r = (X_d/2)$, the displacement at the hoop direction is evaluated by multiplying the radial displacement by the friction coefficient at that interface μ_2 , hence the displacement in the hoop direction (X_{hoop}) is obtained as follows:

$$X_{hoop} = X_a \left(\frac{1 - \mu_1 \tan\left(\frac{\theta}{2}\right)}{\mu_1 + \tan\left(\frac{\theta}{2}\right)} \right) \mu_2 \quad (3)$$

Hoop strain hence can be evaluated by taking the ratio between X_{hoop} and the initial gauge length at both sides $2l_o$ (see Fig. 4) as illustrated in Eq. (4) (Fig. 1).

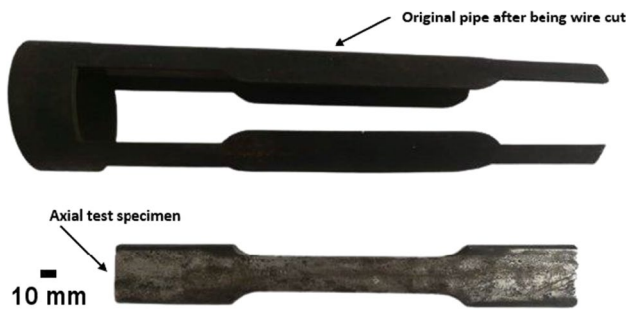
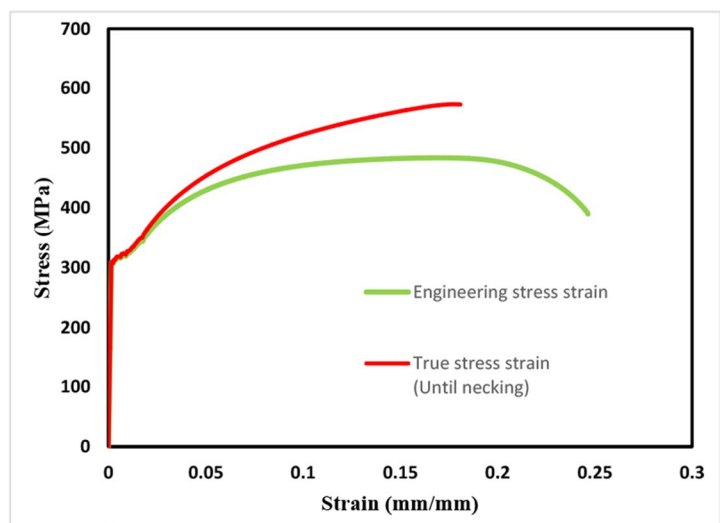


Fig. 2 Axial tensile specimen of the tested pipe

Fig. 3 Engineering and true stress–strain value in the axial direction of the pipe



$$\epsilon_{hoop} = X_a \left(\frac{1 - \mu_1 \tan\left(\frac{\theta}{2}\right)}{\mu_1 + \tan\left(\frac{\theta}{2}\right)} \right) \frac{\mu_2}{2l_o} \quad (4)$$

B Seamless Pressure Pipe), featuring an outer diameter of 73.03 mm and wall thickness of 5.16 mm (pre-machining dimensions). The composition of the material used for the tube is presented in Table 1 [19].

Materials

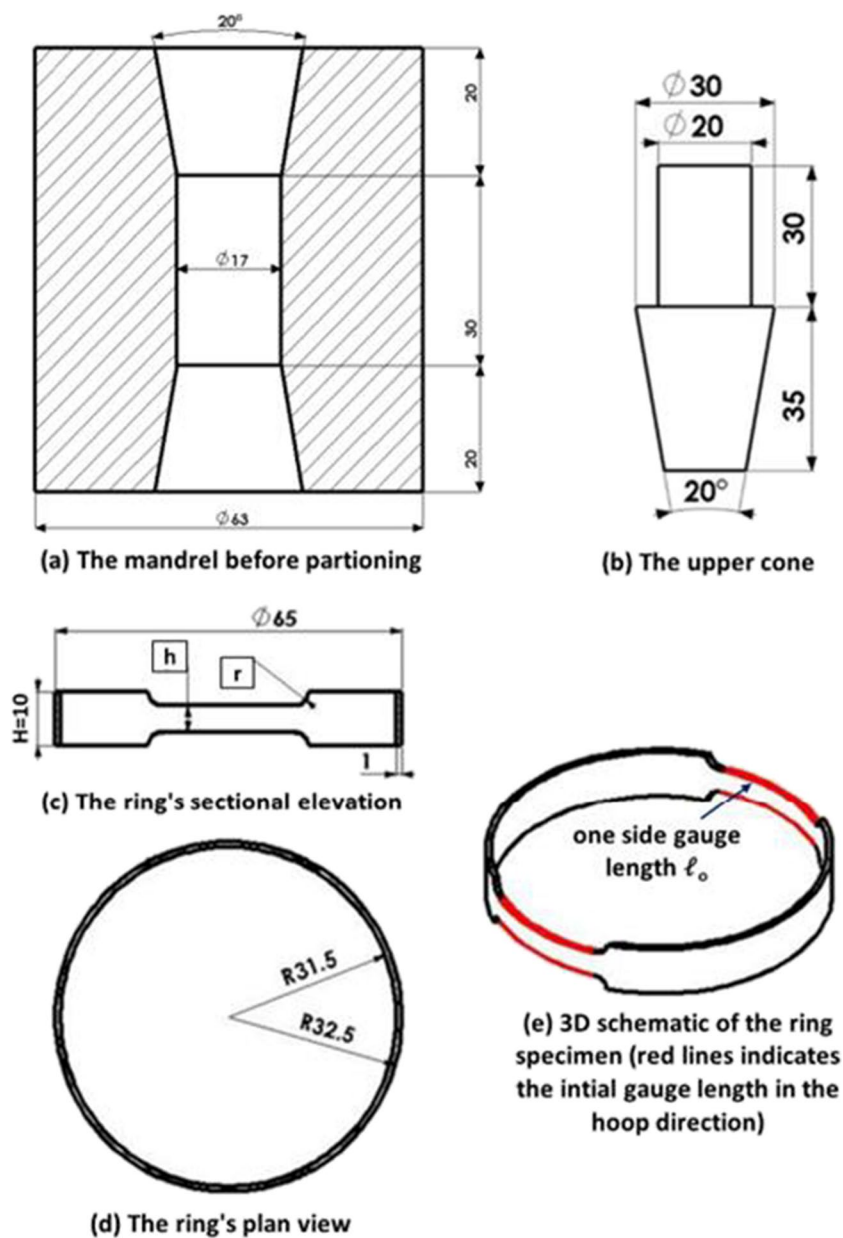
Chemical Composition

The object of investigation in the present study is a seamless round tube with a specification of (ASTM A106 Grade

Tensile Properties

The manufacturer of the pipe has stated that it possesses an Ultimate Tensile Strength (UTS) of 415 MPa and a minimum yield strength of 240 MPa. These parameters were also examined in the current study. Moreover, the test specimens were obtained from the pipe through Electric Discharge Machining (EDM) wire cutting in the axial direction of

Fig. 4 Schematic representation of the testing rig components and the reduced height ring specimen



the pipe, and the dimensions of the test specimen and the cross-head velocity were determined in accordance with the ASTM Standard Test Methods for Tension Testing of Metallic Materials [20]. The axial tensile specimen is shown in Fig. 2. It is also worth mentioning that the pipe's material is isotropic and has the same mechanical properties in both longitudinal and transverse directions [11] which validates the applicability to compare results at any orientation.

The tensile test was performed on three specimens and the median specimen's results for the engineering stress-strain curve in addition to the true stress-strain curve are both clarified in Fig. 3.

Additionally, the components of the bi-cone ring expansion testing rig and the corresponding ring specimen are depicted in Fig. 4. The design of the ring specimen proposed in this study is similar to the axial tensile specimens presented in ASTM E8 tension testing of metallic materials [20], in terms of its geometry and design.

Finite Elements Modelling

The 3D Finite Element Analysis (FEA) was conducted using the commercial finite element method (FEM) package ABAQUS/CAE. A quarter of the model was used in the simulation process due to the symmetry of the model in the XY and XZ planes. For the boundary conditions, a displacement of 10 mm was imposed to a Reference Point (RP) coupled to the cone to move in the negative side of the Y-direction while fixing its movement in both X and Z directions. Certain boundary conditions were added as a portion of the model was used, such as fixing the cone and ring at the XY plane ($u_z = 0$) and fixing the ring and the mandrel from the bottom at the XZ plane ($u_y = 0$), as illustrated in Fig. 5. The assembly of the ring and the mandrel was ensured to keep the separation line between the mandrel parts at the midpoint of the reduced section length (see Fig. 6) as it causes a stress concentration at this region where the specimen is expected to fail. The material of both the cone and the mandrel was defined as elastic steel (Modulus of elasticity $E_{\text{steel}} = 210 \text{ GPa}$ and Poisson ratio $\nu_{\text{steel}} = 0.3$), while the ring material was defined as elastic-plastic material (where the plastic data were obtained from Fig. 3). The element type of C3D8R was used with an element size of 0.5 mm, 2 mm, and 4 mm for the ring, the cone, and the mandrel respectively.

Since the FEA aimed to simulate the experimental procedure, assessing the friction coefficient at the cone/mandrel interface (μ_1) and the mandrel/ring interface (μ_2) presented challenges. Therefore, due to the similar material of both contact bodies and comparable surface roughness of the contact surfaces maintained by sandpapering, a constant value of μ (i.e., $\mu_1 = \mu_2 = \mu$) was assumed throughout the study for simplicity.

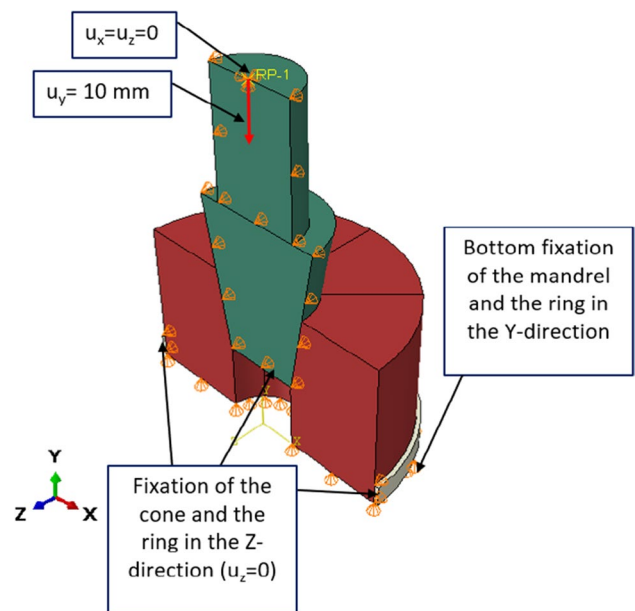


Fig. 5 Boundary conditions applied to the model

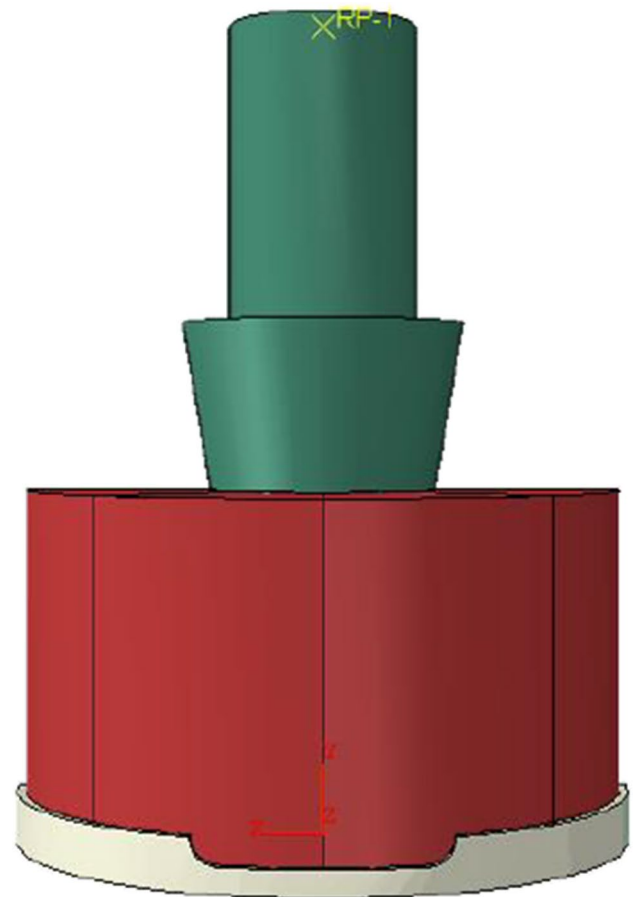
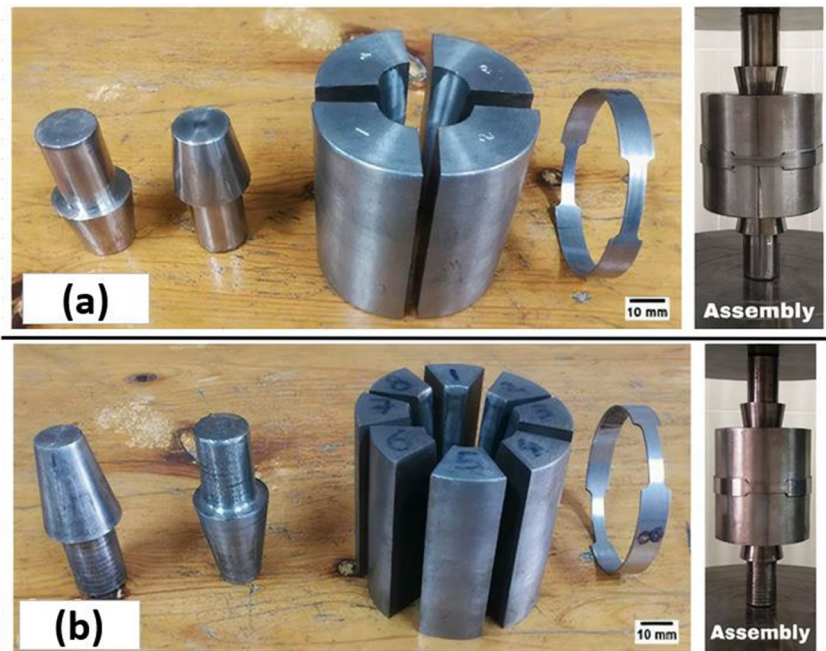


Fig. 6 Back view of the model

Fig. 7 The ring specimen and the two testing rig design components (a) 4-piece and (b) 8-piece



Experimental Work

The experimental tests were carried out using an MTS universal testing machine with a maximum capacity of 100kN. All testing system components (the 8-piece and 4-piece mandrels and the two cones) used were made of steel, and the ring specimen was made of ASTM A106 grade B seamless pipe, as discussed in the materials section. The crosshead speed was set to 2 mm/min. Figure 7 shows the designs of the testing system components, while Fig. 8 demonstrates the assembly of the ring specimen with the testing rig under the testing machine crosshead. Precautions were taken to position the specimen at the mandrel's mid-height. The machine crosshead was gradually pressed down until there was no clearance between both the cones and the mandrel. The applied load and displacement at this point were adjusted to zero. After that, the load and displacement obtained from the test were recorded until the specimen ruptured.

Thus, a total of six experiments were carried out using the 8-piece mandrel and the 4-piece (3 experiments each), and the contact surfaces were ensured to be sandpapered to coincide with the friction assumption. All the assembly precautions performed on the FEA were set to be in the experimental work as well.

Results and Discussion

The failed ring specimens used for the experimental work are demonstrated in Fig. 9. Furthermore, all the rings failed in the tensile mode. This agrees with the failure mode of the dog-bone axial tensile test specimen shown in Fig. 3.

Since the experimental measurements of friction coefficients proved challenging, FEA simulations were used to compare load-extension data with various friction coefficients to experimental measurements. As the conventional true axial tensile test results were used as FEA input to define the elastic–plastic characteristics of the ring's material, and the experimental testing process and FEA simulation followed the same methodology. The load-extension data from FEA simulations with friction coefficients of 0.15, 0.2, and 0.25 at both contact interfaces were compared to experimental test values, as shown in Fig. 10. The FEA results matched well with the testing data (particularly for the 4-piece mandrel design) at a friction coefficient of $\mu = 0.2$. Note that the dimensions (h), (r), and (ℓ_0) in Fig. 4 were 5, 2.5, and 20.32 mm, respectively.

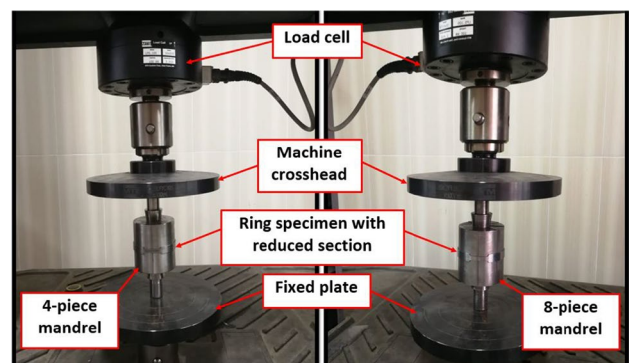


Fig. 8 Assembly of the ring specimen with the 4 and 8-piece mandrel in the test machine

For further verification of the FEA analysis, the hoop stress–strain data obtained from the FEA model at the specimen’s node with maximum hoop stress (as shown in Fig. 11) were compared with the conventional true stress–strain data. Moreover, the axial load–displacement data for both experimental and simulation results were converted into hoop stress–strain data using Eqs. (1) [14] and (4) for the hoop stress and strain, respectively. The pressure dissipation factor (α) was estimated based on the number of mandrel pieces (n), using the mathematical formula ($\alpha = 4.6546 * n^{-2.453}$) proposed by Abdelgawad et al. [18] for similar experimental conditions. The estimated values

of α for the 4- and 8-piece mandrel designs were 15.5% and 2.8%, respectively.

Figure 12 illustrates the comparison between the true axial stress–strain data and the hoop stress–strain data obtained from the node at the ring's maximum hoop stress for the 8-piece mandrel configuration. The converted axial load–displacement data into stress–strain results through Eqs. (1) and (4) respectively for both FEA and experimental results also showed a good agreement. However, the converted stress data using Eq. (1) lacked a multiplied correlation factor (K), as all curves showed the same trend. Therefore, the correlation factor was estimated using a

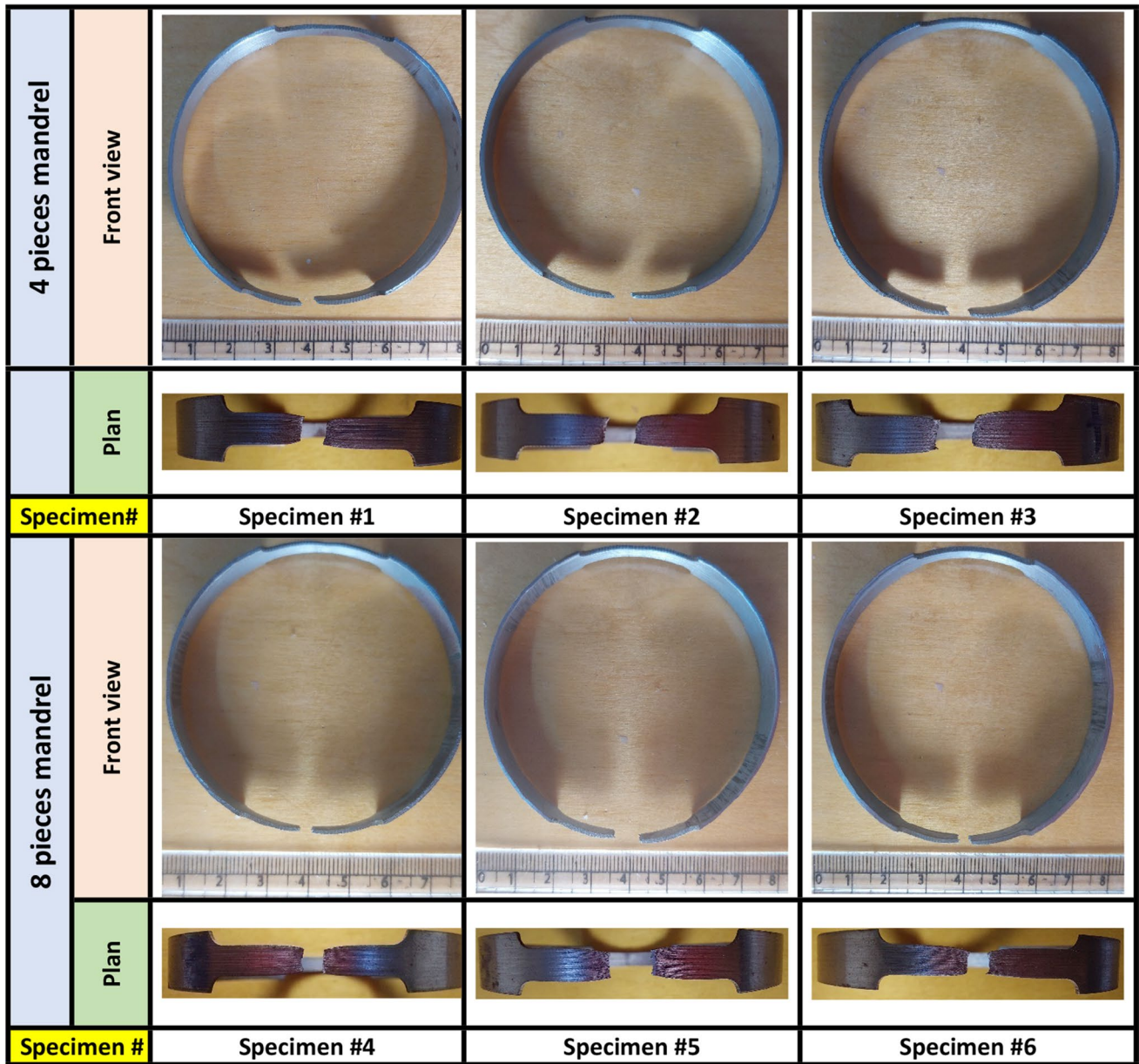


Fig. 9 Tested batch of six-ring specimens using 4- and 8-piece mandrel designs

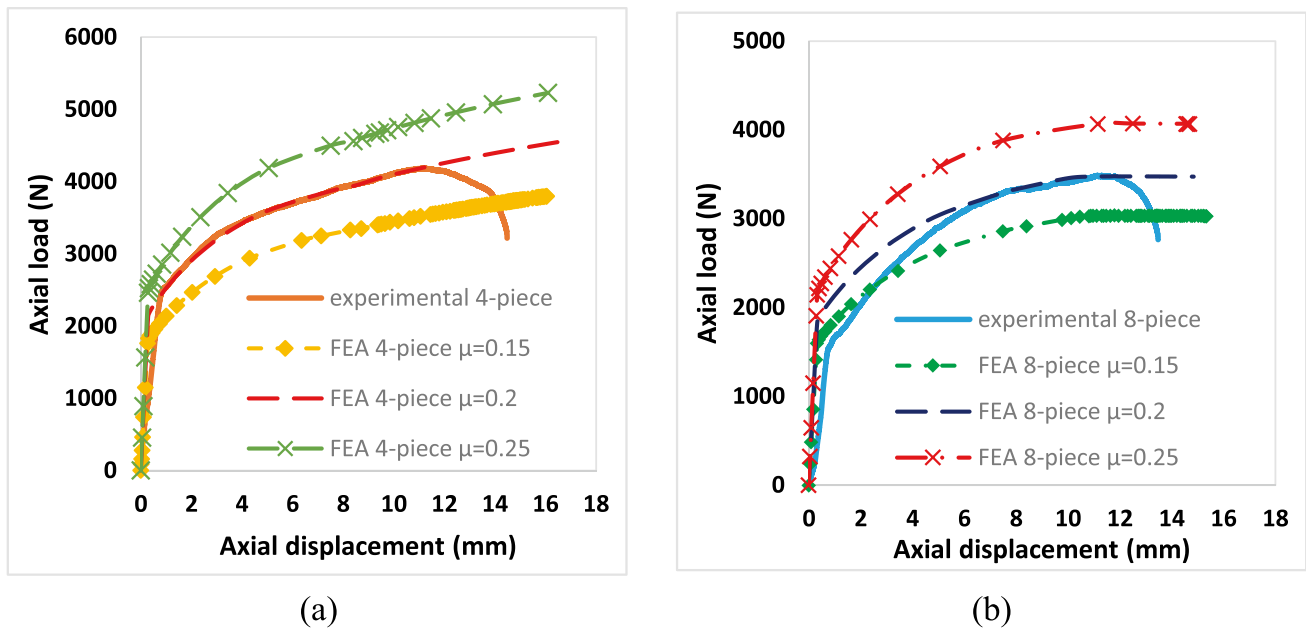


Fig. 10 Comparison between experimental and simulation data for different friction coefficient values (a) 4-piece mandrel and (b) 8-piece mandrel



Fig. 11 The FEA ring specimen with an indication for the node having the maximum hoop stress value

trial-and-error technique to seek the similarity between all the curves, and then Eq. (1) [14] was modified accordingly (see Eq. (5)).

$$\sigma_{\theta} = (1 - \alpha) \frac{FdK}{At} \left(\frac{1 - \mu_1 \tan\left(\frac{\theta}{2}\right)}{\mu_1 + \tan\left(\frac{\theta}{2}\right)} \right) \quad (5)$$

This correlation factor was suggested to be related to the ring's geometry. So, with the aid of the Design of

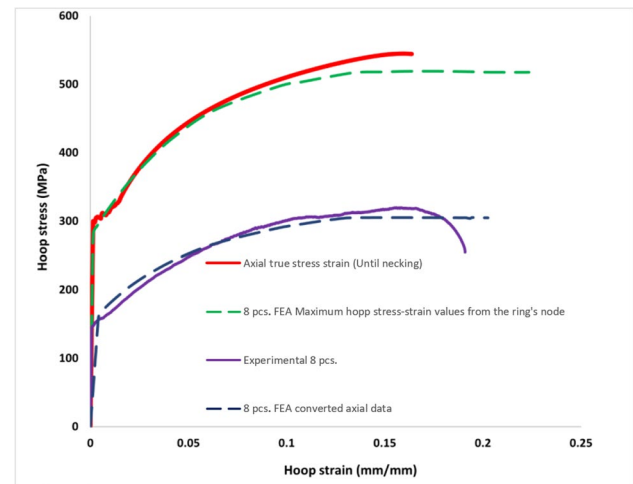


Fig. 12 FEA hoop stress-strain curves vs. conventional axial true test data

Experiment (DoE) 16 simulation models were investigated by changing the reduced section height (h), gauge length (ℓ_o), and their resulting correlation factor (K) as shown in Table 2. It is also worth mentioning that all specimens had a full ring height (H) of 10 mm and a fillet profile of a quarter circle.

The data shown in Table 2 was employed as input data in the Design-Expert statistical software to generate a predictive mathematical model (see Eq. (6)) for estimating the K -factor value based on the dimensions of the reduced section, (h) and (ℓ_o).

Table 2 Specimen geometry used in the Design of Experiment and their corresponding correlation factor (K)

Spc. #	h (mm)	ℓo (mm)	K-Factor
7	1	15.145	7.8
8		18.257	7.4
9		21.38	7.05
10		25.7	6.65
11	3	15.145	2.85
12		18.257	2.75
13		21.38	2.65
14		25.7	2.5
15	5	15.145	1.85
16		18.257	1.8
17		21.38	1.75
18		25.7	1.68
19	7	15.145	1.45
20		18.257	1.42
21		21.38	1.4
22		25.7	1.35

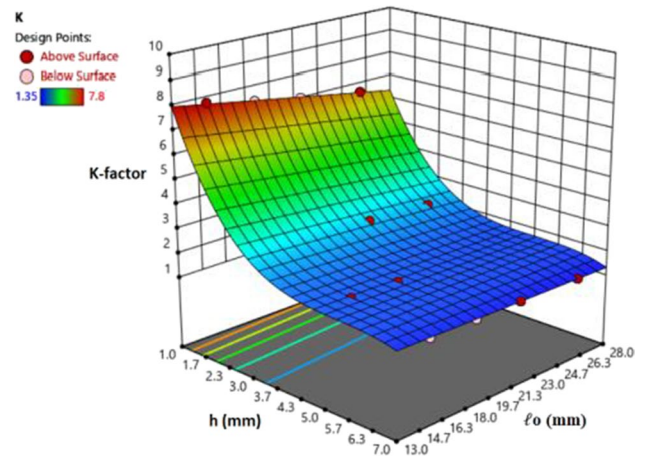


Fig. 14 Surface plotting of the prediction model with further indication of the input data

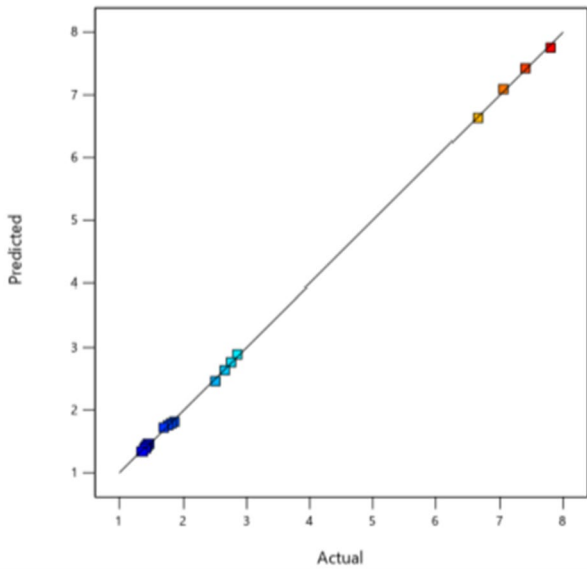


Fig. 13 Predicted vs input (actual) data

$$\begin{aligned}
 K = & 14.865 - 6.555h - 0.15186\ell o \\
 & + 0.05h\ell o + 1.114h^2 - 0.00429h^2\ell o \\
 & - 0.0639h^3
 \end{aligned}
 \tag{6}$$

The predictive ability of the model was verified by comparing the actual data with the predicted values, as illustrated in Fig. 13. Furthermore, Fig. 14 demonstrates the surface plot of the developed equation with an overlay of

the input data points, revealing a greater dependency for the height (h) and the output correlation value (K) when compared to the gauge length (ℓo).

An additional analysis was carried out to confirm the accuracy of the predictive model in comparison with the Finite Element Analysis (FEA) results. Specimens with varying dimensions, as shown in Table 3, were used in this study. The dimensions of the specimens (23, 25, 27, 28, and 30) were designed to maintain a constant ring specimen volume. Figure 15 shows a comparison between the predicted values from the prediction model and the FEA results for the specimens. Interestingly, specimens with the same volume but different height (h) and gauge length (ℓo) values were found to have different correlation factors. This observation supports the idea that the correlation factor (K) is dependent on the height and gauge length values separately, rather than the overall volume of the specimen.

All specimens used in the experimental study had the same dimensions of h = 5 mm, r = 2.5 mm, ℓo = 20.32 mm, and H = 10 mm, which resulted in a correlation factor K of 1.77 based on Eq. 6. The axial load–displacement data obtained from both the experimental and simulation results were converted into stress and strain using Eqs. (5) and (4), respectively. The obtained data were then plotted in Fig. 16 against the reference conventional true axial stress–strain curve. The comparison showed that the data obtained from the proposed test, in combination with the estimated correlation factor (K) and pressure dissipation factor (α), matched well with the reference curve. This provides strong evidence for the validity of the proposed analytical equations as well as the estimated parameters K and α. Additionally, Fig. 16 showed that the correlation factor is applicable to both mandrel models, regardless of the number of mandrel segmentations.

Table 3 Specimens dimension used in the verification study (shaded cells indicate constant volume specimens)

Sp. #	h (mm)	ℓ_o (mm)	Predicted	FEA	error %
23	7	33.165	1.25	1.3	-4.0
24	7	20.32	1.40	1.4	0.2
25	6	23.525	1.69	1.49	13.3
26	5	20.32	1.77	1.75	1.0
27	5	17.415	1.79	1.78	0.8
28	4	13.145	2.11	2.25	-6.2
29	3	20.32	2.68	2.7	-0.8
30	3	9.79	3.10	3.1	0.1
31	1	20.32	7.20	7.1	1.5

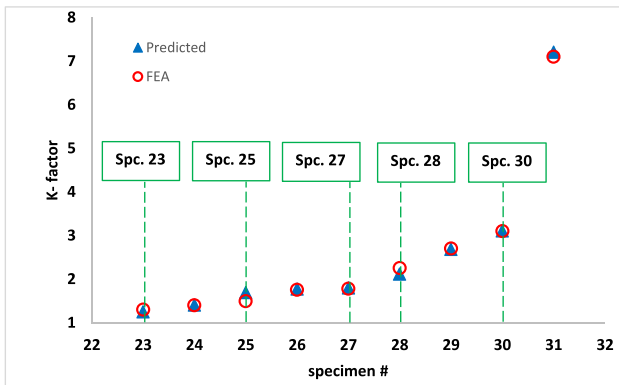


Fig. 15 Predicted vs. FEA results for the K-factor value

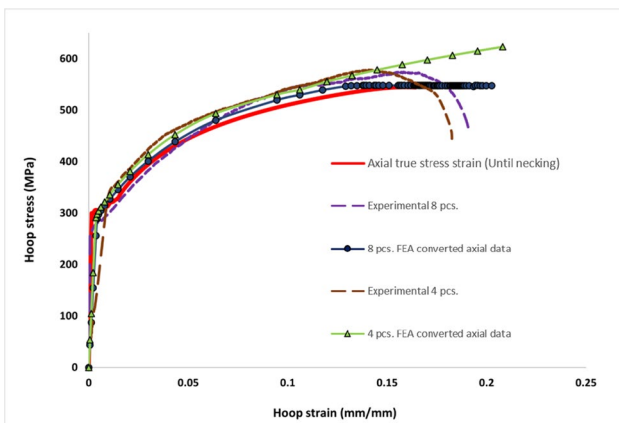


Fig. 16 FEA and experimental hoop stress–strain curves vs. conventional true axial stress–strain

Conclusion and Future Work

In summary, the Bi-cone Mandrel Ring Expansion testing technique is a promising non-conventional method for

evaluating seamless tube material's stress–strain behavior in the hoop direction due to internal pressure. The resulting data matched well with conventional axial tensile test results. Additionally, FEA showed the existence of a correlation factor (K) that is separately dependent on the ring specimen geometry at the reduced section region not the overall volume of the ring specimen. Thus, the key findings of this study can be summarized as follows:

- All ring specimens failed in the same mode as the tensile test specimens (tensile mode).
- Although friction coefficient is hard to evaluate experimentally, it was estimated by comparing the load–displacement curves of the experimental work and the FEA with known values.
- Multiplying the derived hoop stress equation (Eq. (1)) by the correlation factor (K) in case of using a reduced section ring specimen.
- The correlation factor (K) was estimated to be $(K = 14.865 - 6.555h - 0.15186 \ell_o + 0.05h \ell_o + 1.114h^2 - 0.00429h^2 \ell_o - 0.0639h^3)$, considering height (h) as a major effective parameter but not the overall specimen volume.
- Converting axial load–displacement data into stress–strain was effective and had a convenient correlation with the reference standard tensile test.
- The authors propose eliminating strain measurement to predict the material's yield point, which would simplify testing and reduce costs.

Future work for this study includes performing an intensive FEA considering various combinations between the ring geometry parameters to eventually create a full geometric correlation factor table, including full ring height (H), ring diameter (d), and thickness (t), with further experimental verification for different materials either isotropic as presented or anisotropic to seek the validity of the K -factor.

Appendix

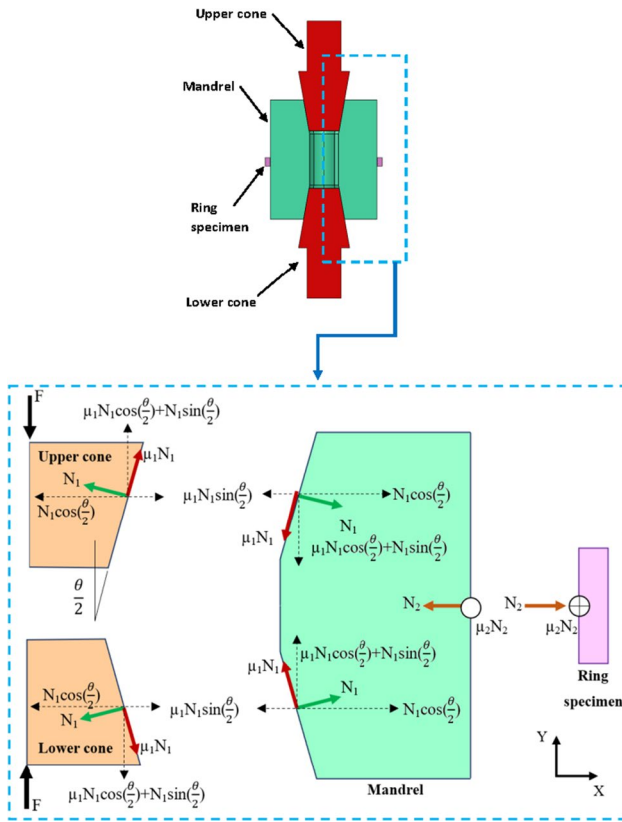


Fig. 17 Force analysis on the testing rig components

Through the free body diagram demonstrated in Fig. 17, the equilibrium of forces acting on the upper cone in the Y-direction are described in Eq. (7). by rearrangement, the value of N_1 could be evaluated through Eq. (8).

$$F - \mu_1 N_1 \cos\left(\frac{\theta}{2}\right) - N_1 \sin\left(\frac{\theta}{2}\right) = 0 \quad (7)$$

$$N_1 = \frac{F}{\mu_1 \cos\left(\frac{\theta}{2}\right) + \sin\left(\frac{\theta}{2}\right)} \quad (8)$$

Taking the same principle but in the X-direction (see Eq. (9)), and by substituting the value of N_1 (Eq. (8)) and rearranging the equation, the radial force acting on the inner surface of the ring N_2 is obtained by Eq. (10).

$$2N_1 \cos\left(\frac{\theta}{2}\right) - 2\mu_1 N_1 \sin\left(\frac{\theta}{2}\right) - N_2 = 0 \quad (9)$$

$$N_2 = 2F \left(\frac{1 - \mu_1 \tan\left(\frac{\theta}{2}\right)}{\mu_1 + \tan\left(\frac{\theta}{2}\right)} \right) \quad (10)$$

Thus, the force component acting in the tangential (hoop) direction of the ring specimen is obtained by multiplying the value of the radial component (N_2) by the friction coefficient (μ_2) which causes the hoop stress on the ring specimen. This analysis was previously performed and published by the authors [17, 18].

Nomenclature d [mm]: Inner diameter of the ring specimen; E_{Steel} [GPa]: Modulus of elasticity of Steel; F [N]: External applied force to the cones; P [MPa]: Actual internal pressure; P' [MPa]: Nominal pressure on the ring inner surface; H [mm]: Height of the ring specimen; h [mm]: Reduced region height; n : Number of mandrel pieces; E_{steel} : Elastic modulus of steel; θ [°]: Taper angle of the cone and of the mandrel tapered hole; K : Hoop stress correlation factor; r [mm]: Reduced region fillet radius; N_1 [N]: Normal force acting on the mandrel inner surface; α : Pressure dissipation factor.; t [mm]: Wall thickness of the ring specimen; ν_{Steel} : Poisson ration of Steel; σ_{θ} [MPa]: Hoop stress; μ_1 : Coefficient of friction between the cone and the mandrel surfaces; μ_2 : Coefficient of friction between the ring and the mandrel surfaces; X_{hoop} [mm]: Displacement in the hoop direction; X_d [mm]: Diametral displacement; X_r [mm]: Radial displacement; X_a [mm]: Axial displacement; A [mm²]: Internal circumferential area; ℓ_o [mm]: Reduced region length; ϵ_{hoop} : Hoop strain; N_2 [N]: Normal force acting on the ring inner surface

Acknowledgements The authors acknowledge the Deanship of Faculty of Engineering- Port Said University for their support throughout this work.

Authors' Contributions All authors have contributed equally to this work.

Funding Open access funding provided by The Science, Technology & Innovation Funding Authority (STDF) in cooperation with The Egyptian Knowledge Bank (EKB). The authors did not receive support from any organization for the submitted work.

Data Availability The raw testing data is available upon request.

Declarations

Ethics Approval The authors declare that this work agrees with the mentioned ethics standard.

Consent to Participate / Publication All authors affirm their equal participation in the work and have no publishing conflict.

Conflicts of Interest/Competing Interests All authors certify that they have no affiliations with or involvement in any organization or entity with any financial interest or non-financial interest in the subject matter or materials discussed in this manuscript.

Open Access This article is licensed under a Creative Commons Attribution 4.0 International License, which permits use, sharing, adaptation, distribution and reproduction in any medium or format, as long as you give appropriate credit to the original author(s) and the source, provide a link to the Creative Commons licence, and indicate if changes were made. The images or other third party material in this article are included in the article's Creative Commons licence, unless indicated otherwise in a credit line to the material. If material is not included in the article's Creative Commons licence and your intended use is not permitted by statutory regulation or exceeds the permitted use, you will need to obtain permission directly from the copyright holder. To view a copy of this licence, visit <http://creativecommons.org/licenses/by/4.0/>.

References

1. ASTM A106 Grade B Pipe | American Piping Products. <https://www.amerpipe.com/steel-pipe-products/carbon-pipe/a106-grade-b/>. Accessed 15 Aug 2022
2. Ktari Z, Leitão C, Prates PA, Khalfallah A (2021) Mechanical design of ring tensile specimen via surrogate modelling for inverse material parameter identification. *Mech Mater* 153:103673. <https://doi.org/10.1016/j.mechmat.2020.103673>
3. Frolov AS, Fedotov IV, Gurovich BA (2021) Evaluation of the true-strength characteristics for isotropic materials using ring tensile test. *Nucl Eng Technol* 53:2323–2333. <https://doi.org/10.1016/j.net.2021.01.033>
4. Gurovich BA, Frolov AS, Fedotov IV (2019) Improved evaluation of ring tensile test ductility applied to neutron irradiated 42XNM tubes in the temperature range of (500 e 1100) C. *Nucl Eng Technol*. <https://doi.org/10.1016/j.net.2019.11.019>
5. Yoon J, Kim J, Kim H et al (2017) Calibration of hoop stress in ring tensile test with Zircaloy-4 tube. *J Mech Sci Technol* 31:4183–4188. <https://doi.org/10.1007/s12206-017-0815-8>
6. Barsoum I, Al Ali KF (2015) A procedure to determine the tangential true stress-strain behavior of pipes. *Int J Press Vessel Pip* 128:59–68. <https://doi.org/10.1016/j.ijpvp.2014.11.002>
7. Khalfallah A, Ktari Z, Leitão C, Fernandes JV (2021) New mandrel design for ring hoop tensile testing. *Exp Tech* 45:769–787. <https://doi.org/10.1007/s40799-021-00462-4>
8. Saber M, Ali B (2021) On the determination of material mechanical properties of St 37 steel pipes using O-Ring specimens. *Exp Tech*. <https://doi.org/10.1007/s40799-021-00455-3>
9. Sultan HM, Othman G, Nassef A (2022) Numerical analysis of full deformation behavior study of pipes material using ring elongation testing technique. *Port-Said Eng Res J* 26(3):146–159. <https://doi.org/10.21608/psrj.2022.126849.1171>
10. Calaf-Chica J, Martínez-Peña J, Bravo Díez PM, Preciado Calzada M (2022) Ring Hoop Tension Test for yield strength estimation: numerical analysis for a novel correlation method and applicability for mechanical testing of tubes and pipes. *Mech Mater* 169:104295. <https://doi.org/10.1016/j.mechmat.2022.104295>
11. Sultan M, Nassef A, Abdunaser G, Saber M (2023) A novel procedure to determine the hoop mechanical properties of pipe materials using ring elongation testing technique. *Int J Press Vessel Pip* 205:105001. <https://doi.org/10.1016/j.ijpvp.2023.105001>
12. Laterreur V, Ruel J, Auger FA et al (2014) Comparison of the direct burst pressure and the ring tensile test methods for mechanical characterization of tissue-engineered vascular substitutes. *J Mech Behav Biomed Mater* 34:253–263. <https://doi.org/10.1016/j.jmbbm.2014.02.017>
13. Seok C, Bae B, Koo J, Murty KL (2006) The properties of the ring and burst creep of ZIRLO cladding. *Eng Fail Anal* 13(3):389–397. <https://doi.org/10.1016/j.engfailanal.2005.02.009>
14. Jiang H, Wang J-AJ (2014) Methodology for mechanical property testing of fuel cladding using an expanding plug wedge test. *J Nucl Mater* 446(1–3):27–37. <https://doi.org/10.1016/j.jnucmat.2013.11.026>
15. Jiang H, Wang J-AJ (2018) Development of cone wedge ring expansion test to evaluate mechanical properties of clad tubing structure. *Prog Nucl Energy* 108:372–380. <https://doi.org/10.1016/j.pnucene.2018.06.015>
16. Jiang H, Wang JJ (2018) Progress in nuclear energy development of cone-wedge-ring-expansion test to evaluate the tensile HOOP properties of nuclear fuel cladding ☆. *Prog Nucl Energy* 108:372–380. <https://doi.org/10.1016/j.pnucene.2018.06.015>
17. Saber M, Chouikhi H (2021) Development of the bicone mandrel ring expansion test to evaluate the hoop stress in extruded aluminum tubes. *Exp Mech*. <https://doi.org/10.1007/s11340-021-00692-y>
18. Abdelgawad K, Nassef A, Eraky MT (2022) Analytical and numerical study of the ring expansion testing technique. *Mater Perform Charact* 11:113–127. <https://doi.org/10.1520/MPC20210142>
19. ASTM A106 Pipe Specifications | American Piping Products. <https://www.amerpipe.com/steel-pipe-products/carbon-pipe/a106/a106-specifications/>. Accessed 25 Mar 2022
20. ASTM E8 (2010) ASTM E8/E8M standard test methods for tension testing of metallic materials 1. *Annu B ASTM Stand* 4:1–27. <https://doi.org/10.1520/E0008>

Publisher's Note Springer Nature remains neutral with regard to jurisdictional claims in published maps and institutional affiliations.